Stability of reinforced earthen dams: Insights from centrifuge model tests

B.V.S. Viswanadham
Indian Institute of Technology Bombay, Mumbai, India, viswam@civil.iitb.ac.in

P. Kumar
New York University Abu Dhabi, Abu Dhabi, United Arab Emirates, pankajkumar@nyu.edu

ABSTRACT: In the present study, the performance of a small-scale reinforced earthen dam with upstream water impoundment was investigated using geotechnical centrifuge modeling. The model, representing a prototype dam height of 7.2 meters, was tested at 40g to evaluate the effect of reinforcement (length-to-height, L_R/H ratio = 0.5) on overall stability and seepage behavior, in comparison with an unreinforced counterpart. While both models had identical horizontal drainage provisions, the reinforcement length was varied to isolate their effects under static hydrostatic loading conditions. The model dams were instrumented with porewater pressure transducers (PPTs) and linear variable differential transformers (LVDTs) to monitor internal pore pressures and surface settlements, respectively, during reservoir filling, steady seepage, and inertial loading. Seismic demand was simulated using a tilt-induced pseudostatic inertial loading approach, representing a first-order approximation of earthquake-induced body forces. Front-view images of the models were recorded using an onboard digital camera, and processed to quantify slope deformations and surface displacements over time. The model with reinforcement achieved a more stable hydraulic regime and maintained structural integrity throughout the test. The study highlights the critical role of reinforcement layers in improving the static performance and pseudostatic seismic stability of earthen dams and provides valuable insights for the design of safer and more resilient embankment structures.

1 INTRODUCTION

Earthen dams and levees remain essential components of water-retention and flood-control infrastructure, yet their performance is closely governed by seepage-induced softening and deformation under sustained reservoir loading or seismic loading. Small to medium earthen dams or embankments with mild to steep slopes, in particular, are vulnerable to elevated pore-water pressures and downstream slope instability when subjected to prolonged impoundment or additional inertial demands. While internal drainage systems can lower phreatic surfaces, they do not directly enhance the mechanical resistance of the dam body (Kumar and Viswanadham, 2023).

Reinforcement using geogrids has gained prominence in slopes (Varuso et al. 2005) and retaining structures (Deng et al. 2025), where tensile resistance and soil-geosynthetic interaction improve deformation control and delay failure mechanisms (Jayanandan and Viswanadham, 2023). Geogrid reinforcement offers a viable means to improve embankment stability by providing tensile confinement, restricting lateral soil movement, and delaying the onset of shear deformation. Numerical studies have suggested potential benefits in improving static and seismic stability and reducing deformations (Yu et al., 2011; Lu et al., 2024), yet their effectiveness under coupled hydraulic-mechanical loading conditions is not well established due to limited experimental evidence at representative stress levels.

Centrifuge modeling has proven effective for studying seepage, deformation, and failure mechanisms in earthen dams because it replicates prototype stresses and hydraulic gradients (Ubilla et al., 2008; Singh et al., 2019; Kumar and Viswanadham, 2024). Recent centrifuge investigations have explored the effect of drainage system in earthen dams and levees (Viswanadham et al. 2025), but systematic evaluation of geogrid reinforcement under reservoir impoundment and inertial loading remains an important research need. This study employs high-g centrifuge tests to evaluate how geogrid reinforcement influences the structural performance, pore-pressure evolution, deformation patterns, and global stability in a small earthen dam under reservoir filling and inertial loading.

2 CENTRIFUGE MODELLING OF REINFORCED EARTHEN DAM

Centrifuge modelling of earthen dams relies on the principle that, at an elevated gravity level N, the stress field within a small-scale model reproduces that of the full-scale prototype. Accordingly, all linear geometric dimensions (dam height, crest width, internal drain length, and reinforcement length) scale as $1/N$, while self-weight stresses scale proportionally with N. Relevant scaling laws are summarised in Table 1. Hydraulic processes follow well-defined similitude constraints: the coefficient of permeability scales as $k_m = Nk_p$, porewater pressures remain unscaled, and the characteristic times for reservoir filling and seepage evolve as $1/N^2$. These relationships ensure that phreatic surface development, transient pore-pressure dissipation, and steady-state flow patterns match prototype behavior.

Table 1. Summary of scaling laws.

Parameter	Scale factor (Model/Prototype)
Dam height (m)	1/N
Side slopes (°)	1
Unit weight (kN/m^3)	N
Stress (kN/m^2)	1
Seepage time (s)	1/N^2
Coeff. of permeability (m/s)	N
Force (kN)	1/N^2
Seismic coefficient	1
Transmissivity (m^2/s)	1
Permittivity (1/s)	1
Tensile load (kN/m)	1/N
Secant modulus (kN/m)	1/N

In the pseudostatic method, earthquake shaking is represented by an equivalent constant horizontal acceleration acting throughout the soil mass. This approach is widely adopted in embankment dam design (Seed and Martin, 1966; Kramer, 1996) for estimating yield acceleration and global stability. The approach is analogous to determining the seismic coefficient corresponding to incipient failure in Newmark-type sliding analyses. In the present centrifuge setup, tilting induces a body force equal to g·sinα, which is statically equivalent to a horizontal seismic acceleration a_h = g·tanα (here α is the inclination angle of the base of the soil model relative to the horizontal plane). The maximum achievable α is 18°. Therefore, K_H = tanα represents the horizontal seismic coefficient applied uniformly throughout the model and remains scale-independent, while the resulting inertial forces scale as $1/N^2$.

For geogrid-reinforced models, tensile load and secant stiffness must be reduced by $1/N$ while preserving strain compatibility, interface friction angle, transmissivity, and permittivity to maintain realistic reinforcement-soil interaction. Together, these scaling laws allow the centrifuge model to replicate the coupled hydraulic-mechanical response of a reinforced earthen dam under reservoir impoundment and inertial loading with high fidelity.

The centrifuge model dam was constructed using a silty sand mixture formulated to replicate the hydraulic and mechanical behavior of typical embankment soils at prototype stress levels. A blend of locally available fine Goa sand (sp. gr. = 2.67, D_{10} = 0.09 mm, D_{50} = 0.17 mm, C_u = 2, C_c = 1.2) and commercially sold kaolin clay (sp. gr. = 2.47, LL = 41%, PL = 27%) was adopted, mixed in a 4:1 ratio by dry mass. The model soil exhibited a specific gravity of 2.62, a maximum dry unit weight of 19.7 kN/m³ (standard proctor), and an optimum moisture content of about 7.5% (standard proctor). Figure 1 depicts the particle size distribution of the model soil. The non-plastic model soil had a liquid limit of 14%. Consolidated undrained triaxial tests yielded an effective friction angle of 33° and an effective cohesion of 5 kPa arising from the kaolin fraction. The coefficient of permeability, determined from falling-head tests (BIS 2720: Part 17), was on the order of 1×10^{-6} m/s (model dimensions). Fine sand having coefficient of permeability of 1×10^{-4} m/s was also used for drainage layers to maintain consistent hydraulic connectivity. Table 2 depicts the summary of physical parameters.

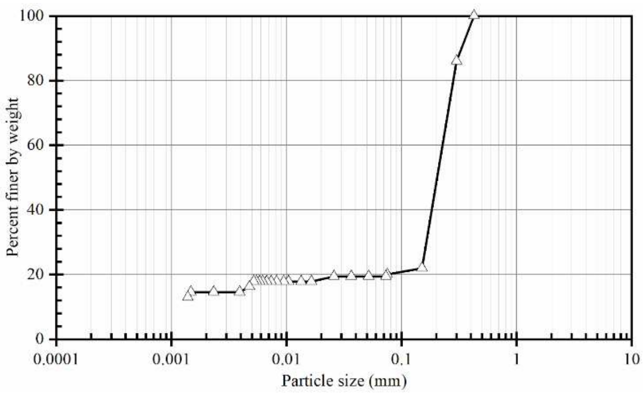

Figure 1. Particle size distribution for the model soil

For the model geogrid (polyester, polyvinyl chloride) with percentage of open area of 97.43%, the wide-width tensile tests on 0.6 mm thick (at 2 kPa) specimen showed an ultimate tensile load of 0.93 kN/m, an ultimate strain of 19.8%, and a secant stiffness (5% strain) of 7.8 kN/m along the cross-machine direction, which was aligned with the reinforcement length during placement. Modified direct shear tests yielded a soil-geogrid interface friction angle of 29.6°, confirming adequate interaction for reinforced embankment modelling. For the reinforced model, the reinforcement length-to-dam height ratio is taken 0.5.

Table 2. Summary of physical parameters.

Parameter	Model (Prototype)
Geometry related	
Dam height (m)	0.18 (7.2)
Side slopes (°)	45 (45)
Soil mix related	
Max. dry unit wt. (kN/m^3)	19.7 (788)
Cohesion (kN/m^2)	5 (5)
Coeff. of permeability (m/s)	10^{-6} (40×10^{-6})
Geogrid related	
Length (m)	0.09 (3.6)
Transmissivity (m^2/s)	2×10^{-5}
Permittivity (1/s)	11.5
Tensile load (kN/m)	0.93 (37.2)
Secant modulus (kN/m)	7.8 (312)

3 MODEL TEST PACKAGE AND MODEL PREPARATION

A tilt-table-based simulator was specially designed to generate hybrid loading conditions (reservoir filling, seepage, and inertial effects) on earthen dam models under elevated gravity in a geotechnical centrifuge. Its design philosophy, operational mechanism, components, and limitations are detailed in Kumar and Viswanadham (2022). The setup incorporates a screw-jack-driven helical gear train for vertical actuation, a swivel assembly with pin and needle-roller bearings for translational motion, and a hinge assembly enabling rotation, as shown in Figure 2. Earthen dam models are placed in an aluminium strongbox (950×250×350 mm) supported within a protective side frame. The complete test package, including the instrumented model, is mounted on the centrifuge's swing basket. Experiments are conducted using the 4.5-m radius large beam geotechnical centrifuge at IIT Bombay (Chandrasekaran 2001).

Centrifuge tests are performed at 40g on the earthen dam models 180 mm high with a 112.5 mm crest width, 45° upstream and downstream side slopes, and a 50 mm impervious base. Two model tests are conducted, namely T1 representing an unreinforced dam section and T2 corresponding to a reinforced dam section. The models are constructed using moist soil compacted in six layers of equal thickness at maximum dry unit weight (MDU) and optimum moisture content. Although field dams are often compacted to approximately 95% of MDU, adoption of 100% MDU in the centrifuge model was intended to minimize variability in void ratio, shear strength, and permeability between repeated tests. Each layer was placed using the pre-weighed soil mass and compacted using a standardized compaction procedure. The thickness of each layer was verified using a scale to ensure uniformity, and samples were taken to verify water content before proceeding with the next placement layer. After each soil layer, the geogrid reinforcement (length-to-height, L_R/H ratio = 0.5, no. of geogrid layers = 5) was placed. Furthermore, L-shaped plastic markers made from thin plastic sheets (20 × 10 mm) were embedded after each soil (and geogrid) layer within front elevation and along the inclined slope faces to determine relative displacements with respect to the permanent markers. Since both reinforced and unreinforced models are prepared at the same compaction state, the comparative assessment of reinforcement performance remains unaffected by the absolute compaction level.

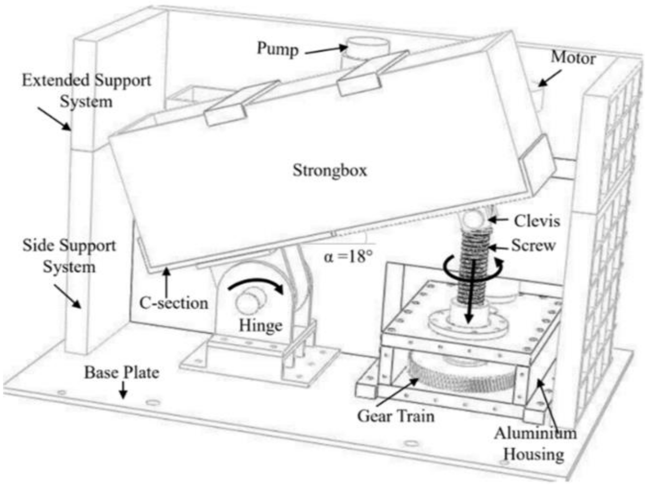

Figure 2. Schematic of the model test package and the inertial loading setup

The downstream toe of the models has been provided with a blanket drain (length-to-dam height ratio 0.5). The instrumentation involved the placement of five PPTs (model: EPB-PW, TE connectivity; accuracy: ±1% FS) at the base of the dam section, and two LVDTS (for vertical displacement; make: Trans-tek Inc., USA; linearity: ±0.5% FS) at the crest of the dam. The schematic layout of the model earthen dam is shown in Figure 3. Finally, the model test package is placed on the centrifuge swing basket.

The centrifuge is initially operated and progressively accelerated to 40g, allowing the model to attain stable equilibrium conditions for 10 minutes (model dimensions), until crest settlement stabilised to less than 0.1 mm/hr. Subsequently, water is introduced into the upstream compartment to achieve the maximum water level (MWL = 0.917H), which is maintained using a standpipe arrangement. This procedure ensures the establishment of steady-state seepage conditions within the dam section. Thereafter, inertial loading is applied to the centrifuge model by actuating the screw jack, producing a controlled tilting rate of δ = 0.7°/min.

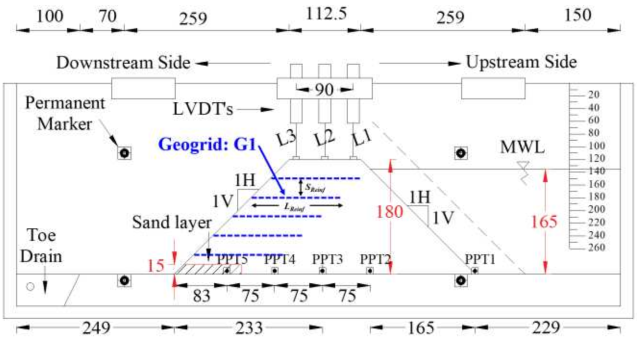

Figure 3. Schematic layout of the reinforced earthen dam model tested at 40g (All dimensions are in mm)

The purpose is to evaluate yield acceleration and global stability under gradually increasing equivalent inertial demand, rather than to reproduce earthquake frequency content or cyclic shaking effects. The test is terminated and the centrifuge is decelerated to normal gravity either upon the observation of distress through onboard video monitoring or transducer responses.

4 ANALYSIS AND INTERPRETATION OF CENTRIFUGE TEST

The overall performance of the reinforced earthen dam was assessed by evaluating its seepage response and deformation behavior. Digital image analysis was conducted using ImageJ (2012) software on selected in-flight images (average resolution 6 pixels/mm) obtained at critical stages of the centrifuge tests, corresponding to significant deformation events. The coordinates of markers prior to water rising serve as reference points for relative movements. These images were analyzed to determine face deformations and displacement contours of the dam section under inertial loading conditions. Hereafter, all physical quantities (pore pressures, seepage time, deformation, etc.) are now expressed in prototype dimensions. Figure 4 depicts the variation of porewater pressure measured for both unreinforced and geogrid-reinforced earthen dam models with time elapsed from the onset of upstream filling in prototype dimensions. PPT1 recordings indicate that both dam models experienced a nearly identical and uniform rise in upstream water level. An average flood rise rate of 0.33 m/day was achieved in both models. The maximum upstream water pressures recorded were 66 kPa and 64 kPa for models T1 and T2, respectively. The high flood level (HFL) was reached after approximately 20 days of seepage in all models. The water level was maintained for up to 40 days of seepage to ensure steady-state conditions. PPT2 recordings were also nearly identical for both models, further confirming the similarity in hydraulic response. The pore water pressures measured at the toe region by PPT4 and PPT5, which varied between 4 and 6 kPa in both models, clearly demonstrate the effectiveness of the horizontal drain in dissipating excess pore water pressure. Both models incorporating internal drainage layers exhibited steady-state seepage conditions during the flooding stage and remained stable for up to 40 days of seepage without any significant distress.

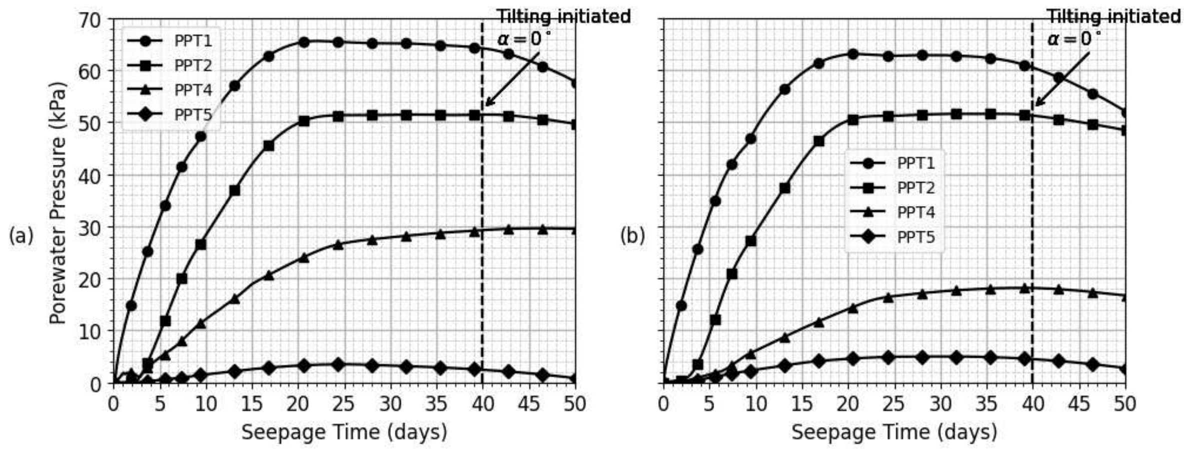

Figure 4. Variation of porewater pressure in the earthen dam during steady-state seepage conditions: (a) Unreinforced Section and (b) Reinforced Section

Further, as the upstream reservoir was impounded, a small amount of vertical settlement was observed at the crest of the earthen dam, as illustrated in Figure 5. Vertical settlements were measured using LVDTs: L1 and L3, installed at distances of 1.0 m and 3.4 m, respectively, from the upstream edge of the dam crest. During the steady-state seepage condition, the recorded settlements ranged from approximately 0.008 m to 0.015 m and subsequently stabilised upon attainment of the maximum water level. However, upon the initiation of inertial loading (after 40 days of seepage), the crest of the unreinforced dam remained largely intact, with failure predominantly confined to the downstream slope, resulting in negligible additional vertical settlement at the crest.

In contrast, the reinforced model T2 experienced pronounced deformation at the crest, with a maximum vertical settlement of about 3.5 m recorded by displacement transducer L3 located toward the downstream side. It should be noted that the unreinforced model T1 failed at a relatively early stage, at an inclination angle (α) of approximately 11.2°, and to preserve the overall geometry of the model, appropriate corrective measures were undertaken and the centrifuge test was terminated. In comparison, the reinforced model T2 withstood significantly higher inertial loading and failed much later at α ≈ 16.2°, exhibiting a catastrophic mode of failure.

Figure 6 clearly illustrates the contrasting deformation responses of the unreinforced and reinforced dam sections under inertial loading. The unreinforced model exhibits relatively low resultant displacements, mostly confined to the downstream slope, with magnitudes generally limited to about 2-3 m, corresponding to its earlier failure at α ≈ 11.2° (or $K_H = 0.20$). Water supply to the upstream reservoir was terminated immediately upon observation of global instability, thereby preserving the post-failure geometry of the model dam. The displacement field remains localized, indicating a progressive slope instability without significant crest involvement. In contrast, the reinforced section sustains higher inertial loading and fails at a larger horizontal seismic coefficient of $K_H = 0.29$. At failure, the reinforced model shows widespread deformation extending from the downstream slope to the crest, with peak resultant displacements reaching approximately 10 m. This behaviour reflects effective load redistribution and enhanced global stability provided by reinforcement, followed by substantial strain accumulation and a sudden, catastrophic failure mode once the reinforcement capacity is exceeded.

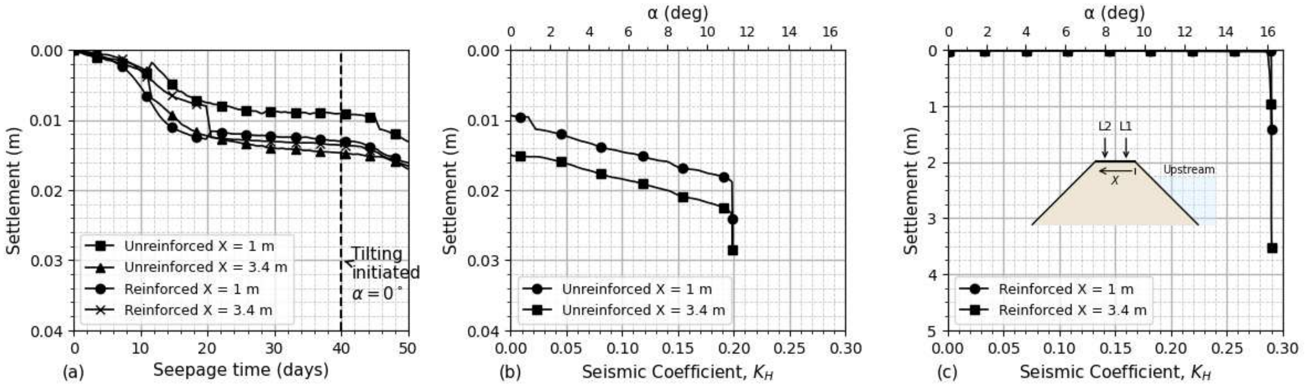

Figure 5. Settlement response recorded by LVDTs at the crest of the earthen dam section: (a) during steady-state seepage condition, (b) during tilting stage for the unreinforced section, and (c) during tilting stage for the reinforced section

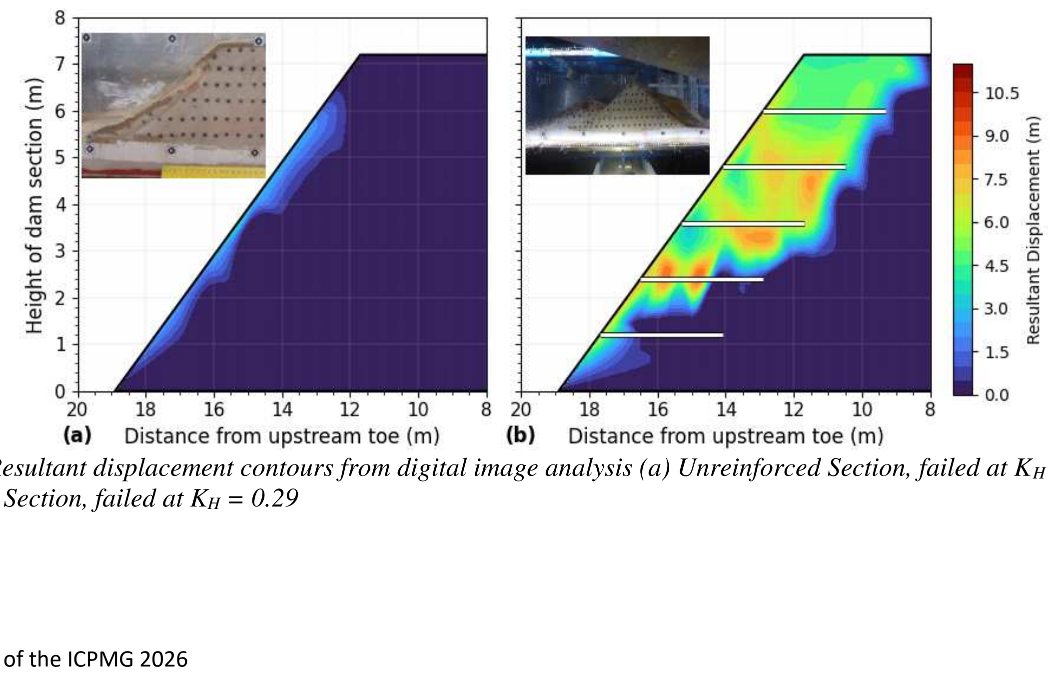

Figure 6. Resultant displacement contours from digital image analysis (a) Unreinforced Section, failed at $K_H = 0.2$ and (b) Reinforced Section, failed at $K_H = 0.29$

5 CONCLUSIONS

This investigation provides rare centrifuge-scale insight into the performance of earthen dams with and without internal reinforcement under steady-state seepage conditions followed by inertial loading. Both models exhibited nearly identical hydraulic responses during reservoir impoundment, attaining steady-state seepage with consistently low toe pore water pressures (4 to 6 kPa), thereby reaffirming the critical role of internal drainage systems in maintaining hydraulic stability. Under inertial loading, the unreinforced dam failed at a relatively low seismic demand ($K_H = 0.20$), with deformation largely confined to the downstream slope and minimal crest involvement.

In contrast, the reinforced dam sustained substantially higher seismic loading ($K_H = 0.29$), demonstrating a pronounced enhancement in global stability. Notwithstanding this improvement, failure of the reinforced configuration was marked by widespread deformation and severe crest settlement, reflecting significant strain accumulation and a sudden, catastrophic collapse once reinforcement capacity was exceeded. These findings underscore that while reinforcement can substantially elevate seismic resistance, it may also alter the failure mechanism and deformation demands, reinforcing the need for performance-based seismic design frameworks that explicitly account for allowable deformations in addition to conventional stability criteria. The pseudostatic approach is employed here to evaluate ultimate stability and deformation capacity under sustained inertial loading. The method does not capture cyclic degradation or dynamic amplification effects, and therefore the results should be interpreted as limit-state stability thresholds rather than full dynamic response predictions.

ACKNOWLEDGEMENTS

The authors gratefully acknowledge the staff of the National Geotechnical Centrifuge Facility (NGCF), Indian Institute of Technology Bombay, India, for their invaluable support and assistance throughout the course of this study.

REFERENCES

BIS 2720: Part 17 (2024). Methods of Test for Soils-Laboratory Determination of Permeability. Bureau of Indian Standards, New Delhi, India.

Chandrasekaran, V.S. (2001). Numerical and Centrifuge Modeling in Soil-Structure Interaction. *Indian Geotechnical Journal*, 31(1): 1-59.

Deng, W., Ding, X., Wang, C., Yang, C., Ren, Z., Ou, Q., Wang, R. (2025). Experimental and numerical analysis of wrapped geogrid-stabilized high-fill embankment: Seismic response and composite reinforcement mechanisms. *Geotextiles and Geomembranes*, 53(6): 1357-1374.

ImageJ (2012). User Guide, version 1.52a. National Institute of Health, USA.

Jayanandan, M. and Viswanadham, B.V.S. (2023). DIA of centrifuge model tests on geogrid reinforced soil walls with low-permeable backfills subjected to rainfall. *Geotextiles and Geomembranes*, 51(4): 36-55.

Kumar, P. and Viswanadham, B.V.S. (2022). Design and Development of Tilt Table-Based in-flight Simulator for Pseudostatic Loading in a Geotechnical Centrifuge. *Geotechnical Testing Journal*, ASTM, 45(5): 936-960.

Kumar, P. and Viswanadham, B.V.S. (2023). Numerical Studies on Seepage-Stability Analysis of Retention-Type Earthen Dams. *Indian Geotechnical Journal*, 53(2): 348-361.

Kumar, P. and Viswanadham, B.V.S. (2024). Studies on the performance of water retention type tailings dams subjected to filling and inertial loading in a geotechnical centrifuge. *Engineering Geology*, 331. DOI: 10.1016/j.enggeo.2024.107412.

Kramer, S.L. (1996). *Geotechnical Earthquake Engineering*, Second edition, Prentice-Hall, Upper Saddle River, New Jersey, USA.

Lu, L., Chen, B., Wang, Z., Wang, S., and Arai, K. (2024). Study on seismic stability and performance of reconstruction embankment using geogrid reinforced soil technology. *Transportation Geotechnics*, 44(1): 1-13. https://doi.org/10.1016/j.trgeo.2023.101148

Seed, H.B., and Martin, G.R. (1966). The Seismic Coefficient in Earth Dam Design. *Journal of the Soil Mechanics and Foundations Division,* ASCE, 92(3): 25-58.

Singh, J., Horikoshi, K., Mochida, Y., and Takahashi, A. (2019). Centrifugal tests on minimization of flood-induced deformation of levees by steel drainage pipes. *Soils and Foundations*, 59(2): 367-379.

Ubilla, J., Abdoun, T., Sasanakul, I., Sharp, M., Steedman, S., Wipawi, V.E., and Zimmie, T. (2008). New Orleans Levee System Performance during Hurricane Katrina: London Avenue and Orleans Canal South. *Journal of Geotechnical and Geoenvironmental Engineering*, ASCE, 134(5): 668-680.

Varuso, R.J., Grieshaber, J.B. and Nataraj, M.S. (2005). Geosynthetic reinforced levee test section on soft normally consolidated clays. *Geotextiles and Geomembranes*, 23(4): 362-383.

Viswanadham, B.V.S., Kumar, P., and Saran, R.K. (2025). Centrifuge modelling of levees with geocomposite chimney drain subjected to flooding. *Geosynthetics International*, 32(2): 257-275.

Yu, Y.M., He, Y.L., and Wu, X.Y. (2011). Aseismic strengthening effect of geogrid in high rockfill dam. *Chinese Journal of Geotechnical Engineering*, 33(9): 1425-1433.